Geomechanics and Engineering, *Vol. 15, No. 2 (2018) 721-728*
DOI: https://doi.org/10.12989/gae.2018.15.2.721

The effect of radial cracks on tunnel stability

Lei Zhou[a], Zheming Zhu[*], Bang Liu and Yong Fan

MOE Key Laboratory of Deep Underground Science and Engineering, College of Architecture and Environment, Sichuan University, Chengdu 610065, China

(Received May 5, 2017, Revised September 28, 2017, Accepted November 29, 2017)

Abstract. The surrounding rock mass contains cracks and joints which are distributed randomly around tunnels, and in the process of tunnel blasting excavation, radial cracks could also be induced in the surrounding rock mass. In order to clearly understand the impact of radial cracks on tunnel stability, tunnel model tests and finite element numerical analysis were implemented in this paper. Two kinds of materials: cement mortar and sandstone, were used to make tunnel models, which were loaded vertically and confined horizontally. The tunnel failure pattern was simulated by using RFPA2D code, and the Tresca stresses and the stress intensity factors were calculated by using ABAQUS code, which were applied to the analysis of tunnel model test results. The numerical results generally agree with the model test results, and the mode II stress intensity factors calculated by ABAQUS code can well explain the model test results. It can be seen that for tunnels with a radial crack emanating from three points on tunnel edge, i.e., the middle point between tunnel spandrel and its top with a dip angle 45°, the tunnel foot with a dip angle 127°, and the tunnel spandrel with 135° with tunnel wall, the tunnel model strength is about a half of the regular tunnel model strength, and the corresponding tunnel stability decreases largely.

Keywords: tunnel; crack; numerical model; tunnel model test; stress intensity factor

1. Introduction

With increasing scale of tunnel constructions in mining and transport engineering, a series of accidents produced in the processes of tunnel excavations have been exposed, such as rock burst and roof fall. Rock usually contains a large number of natural joints or cracks which are distributed randomly around tunnels, and meanwhile, in the process of rock excavation, fragmentation by explosive is a widely applied method in mining and quarrying due to its properties of easy operation, less cost, and high efficiency. Under the action of explosive detonation, blast-induced radial cracks will occur in the surrounding rock (Zhu 2009b) which could largely weaken tunnel stability. It is expected that as crack position differs, the effect extent on tunnel stability and tunnel damage-failure mode should vary, but these are not clear yet, for example, if a radial crack emanating from tunnel roof has more effect than that from tunnel bottom. In order to clearly understand the effect of cracks on tunnel stability and cracked tunnel failure mechanism, it is essential to implement the corresponding experimental and numerical studies so as to obtain a better understanding of the dominant parameters that control tunnel stability.

The issue of tunnel stability has been studied experimentally and numerically by many researchers, and accordingly many significant research results have been published. Research results (Baziar *et al.* 2016, Satıcı *et al.* 2014, Yang and Yan 2015, Yoo 2016, Zhang *et al.* 2017) showed that the existing of faults or cracks have a significant negative influence on the stability and service life of tunnel structures, and they could weaken tunnel stability and cause large engineering disasters. This is because that the excavation of the underground tunnel would destroy the original stress equilibrium conditions, resulting in the stress redistribution around the tunnel, and then induced crack initiation and expansion (Mambou *et al.* 2015). By performing a characterisation study on faults at different scales, and by means of the Hoek-Brown method, Gattinoni *et al.* (2016) estimated fault rock strength, and they pointed out that the distribution of rock faults in a tunnel was the most important factor in the occurrence of rock burst.

Joint's effect on tunnel stability has been investigated by many researchers (Ghorbani *et al.* 2015, Nikadat 2016, Wang *et al.* 2016a). Through a series of two dimensional numerical modeling, Gong *et al.* (2005) pointed out that joint orientation can significantly influence crack initiation and propagation as well as the fragmentation pattern. Huang *et al.* (2013) studied the impact of weak interlayer (joint) on roadway stability by model tests and numerical simulation, and the results showed that the position, dip angle and distance of weak interlayer as well as the thickness are the essential factors for tunnel instability.

Cracks can be considered as a small fault, and the number of cracks are much more than that of the large-size faults in rock materials. Crack positions to a tunnel and crack dimensions play an important role on tunnel stability (Chen 2014, Li *et al.* 2014, Park *et al.* 2012, Sun *et al.* 2013). Wang *et al.* (2012) investigated the influence of

∗Corresponding author, Professor
E-mail: zhemingzhu@hotmail.com
[a]Ph.D Student
E-mail: zhouleittkx@126.com

http://www.techno-press.org/?journal=gae&subpage=7
ISSN: 2005-307X (Print), 2092-6219 (Online)

stress intensity factor on tunnel stability through a photoelastic study, and their test results demonstrated that when crack dip angle is 45° or 135°, the crack tip stress intensity factor is the maximum. Liu *et al.* (2015) investigated the distributions of shear micro-cracks and tensile micro-cracks in a tunnel under compression, and the results showed that shear micro-cracks were predominantly observed at the sidewalls, whereas tensile micro-cracks were dominant at the regions around the tunnel roof. Through model tests and numerical simulation, Zhu *et al.* (2015) investigated the influence of principal stress orientation on the stability of tunnels and cracked tunnels, and the results showed that for tunnels with a radial crack emanating from tunnel spandrel, as the crack angle with the tunnel wall is 135°, the stability of the cracked tunnel is the lowest.

In numerical study, many numerical simulation techniques and methods have been employed. By using finite element method (FEM), Dhawan *et al.* (2002) analyzed the effects of weak zones in rock mass and creation of multiple cavities in the inhomogeneous rock mass. By using hybrid method of FEM and boundary element method (BEM), Lee and Kim (2003) assessed the effect of fault zones under different in-situ stresses. By using RFPA code, Wang *et al.* (2014) simulated the evolution of cracks in three-dimensional space, as well as the heterogeneity of the rock mass by using a discontinuous deformation model, numerical results showed that both the ligament angle and the flaw angle of two pre-existing cracks can affect the uniaxial compressive strength of the specimen and the mechanism of fracture evolution. Huang and Xiao (2010) simulated the construction of a double arch tunnel through a weak interlayer based on Mohr-Coulomb yield criterion by FLAC3D code. Erdi *et al.* (2015) used the limit strain method to analyze the damage process of a circular tunnel, including the damage depths of surrounding rock and the related safety coefficients.

Although many significant results have been published, less attention has been paid to the effect radial cracks emanating from tunnel edge, and the corresponding systematical study result cannot be found. In this paper, the corresponding numerical simulations and model tests are implemented. In the experimental study, cement mortar and sandstone are used to make tunnel models, which are loaded vertically and are confined horizontally. In the numerical study, finite element based code RFPA^{2D} and ABAQUS are employed, and the simulation results are compared with model test results.

2. Tunnel model tests

Faults or cracks may have a significant effect on tunnel stability, and therefore, it is necessary to perform experimental and numerical studies on cracked tunnel failure property. In this study, horseshoe configuration tunnel models are tested, and three types of radial cracks will be considered. The first one is radial cracks emanating from a tunnel roof, and totally there are seven groups of specimens with different dip angle θ (0°, 15°, 30°, 45°, 60°, 75° and 90°) between the crack and horizontal axis, as shown in Fig. 1 (a). The second one is those emanating from the bottom and from the sidewall of tunnels, and the angle between the crack and the tunnel free surface is kept as a constant 45°, as shown in Fig. 1(b). The third one is those emanating from the tunnel foot with different dip angles α (from 15° to 255°, with 15° gradient increment) with tunnel bottom, as shown in Fig. 1(c).

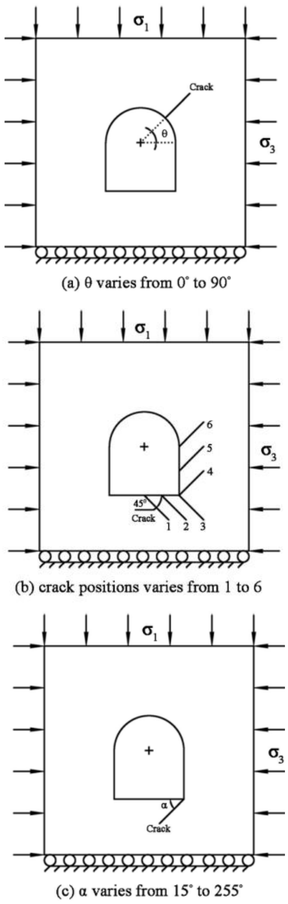

Fig. 1 Sketch of loading conditions and tunnel models with a radial crack emanating from different locations of tunnel edge

Table 1 Material parameters of cement mortar and sandstone tunnel model

Material	Young's modulus E (GPa)	Poisson's ratio u	Density ρ (kg/m^3)	Cohesion c (MPa)	Internal friction angle ψ(°)	UCS (MPa)
Cement mortar	2.95	0.25	2265	1.5	15	8.25
Sandstone	4.2	0.26	2350	2.1	35	22.08

2.1 Tunnel models

The models are square plates measuring 350 mm in length, 350 mm in width and 100 mm in thickness with a centralized small tunnel, which is 60 mm in height and 50 mm in width, and the tunnel's arch consists of a semi-circle and the diameter of the circular arch is 50 mm. The models were made by using two kinds of materials, cement mortar and sandstone. For cement mortar, the ratio of cement:sand:gypsum:water is 1:2.5:0.6:0.45 by weight. The mechanical parameters of cement mortar and sandstone

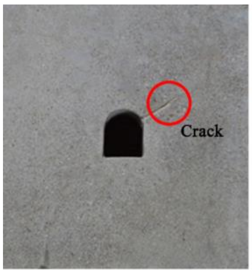

(a) tunnel roof

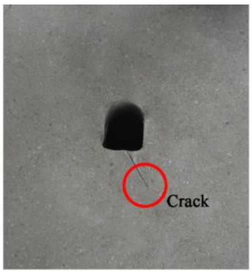

(b) tunnel bottom

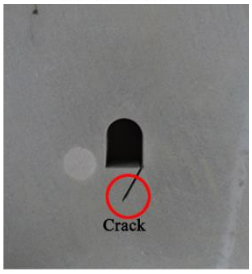

(c) tunnel foot

Fig. 2 Pictures of tunnel models with a radial crack emanating from different locations of tunnel edge

were tested by using prism specimens with dimension 70.7 mm×70.7 mm×70.7 mm, and the results are shown in Table 1.

The pre-crack is 50 mm in length, and for those specimens made by using cement mortar, the cracks were made by using a thin plastic film measuring 0.25 mm in thickness, which was placed inside the tunnel models during the process of casting in a mold until they were loaded. The three types of cracked tunnel specimens are shown in Figs. 2(a), 2(b) and 2(c), respectively. For the sandstone tunnel models, the crack tips were sharpened by a very thin steel saw.

For tunnel models with a radial crack emanating from the tunnel roof, 7 groups of tunnel specimens were made by using cement mortar and sandstone, respectively. For those with a radial crack emanating from the bottom and sidewall, 6 groups of specimens were made by using cement mortar and sandstone, respectively. For those emanating from the tunnel foot, 17 groups of specimens were made by using sandstone. One group specimens without cracks was made for each material, and each group of models consists of three specimens.

2.2 Loading method

Considering the fact of lateral pressure on underground tunnels, on both sides of tunnel models, a confining pressure was loaded by two steel plates, which can made the tunnel models in the state of biaxial compression. One steel plate was loaded by the hydraulic jacks, and the other one was fixed. Before testing, a very small lateral pressure was loaded, and then, the vertical stress (σ_1) was loaded through the Electro-hydraulic servo control device (500T), as shown in Fig. 3, until the tunnel model fails. Based on the lateral deformation is zero, the relationship between the minor principal stress σ_3 in the horizontal direction and the major principal stress σ_1, according to the elastic theory, can be expressed as

$$\sigma_3 = \nu\sigma_1 \tag{1}$$

where ν is Poisson's ratio.

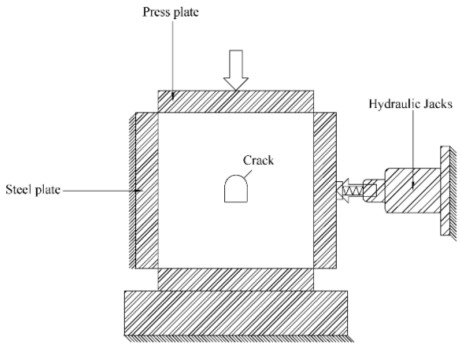

Fig. 3 Sketch of loading device used in this experimental study

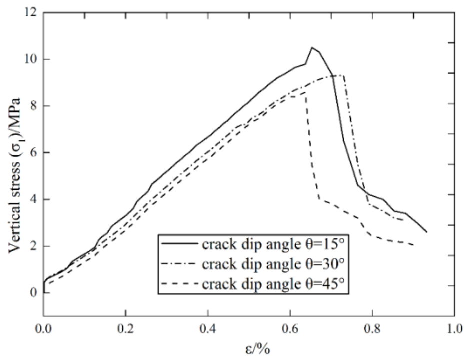

Fig. 4 The stress-strain curves for the tunnel models with a radial crack emanating from tunnel roof with three dip angles

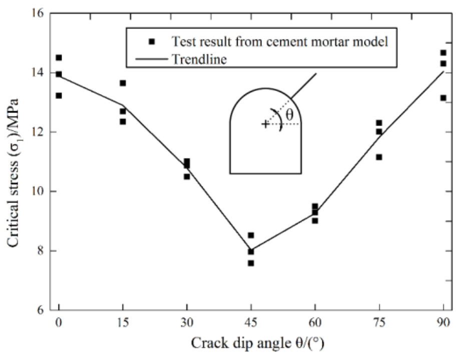

Fig. 5 Testing results of the critical stress σ_1 with different crack dip angle θ for cement mortar tunnel models with a radial crack emanating from the tunnel roof

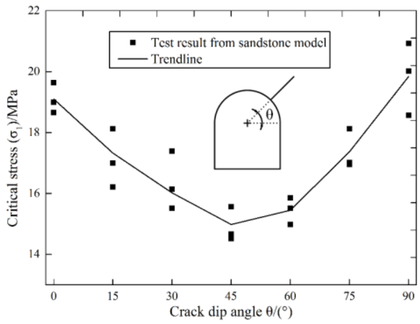

Fig. 6 Testing results of the critical stress σ_1 with different crack dip angle θ for sandstone tunnel models with a radial crack emanating from the tunnel roof

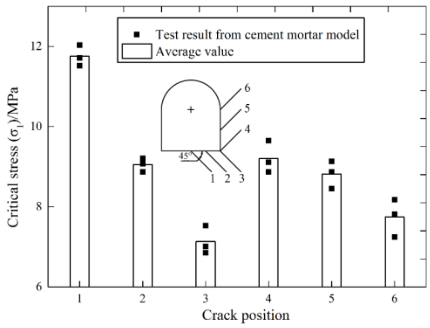

Fig. 7 Testing results of the critical stress σ_1 with different crack positions for cement mortar tunnel models with a radial crack emanating from the bottom and sidewall of tunnel models

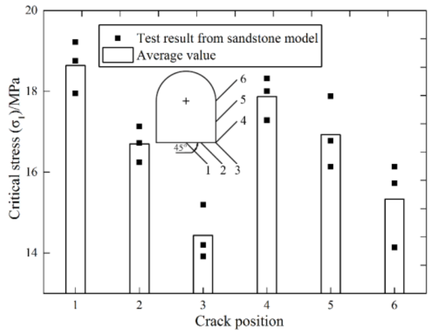

Fig. 8 Testing results of the critical stress σ_1 with different crack positions for sandstone tunnel models with a radial crack emanating from the bottom and sidewall of tunnel models

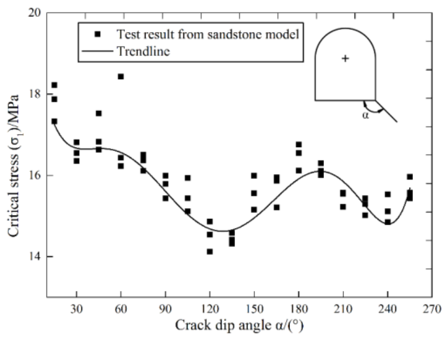

Fig. 9 Testing results of the critical stress σ_1 with different crack dip angles α for sandstone tunnel models with a radial crack emanating from the tunnel foot

In order to decrease the influence of uneven surface, the specimen surfaces were polished by using grinder before loading. The specimen surfaces were also smeared with a kind of lubricant, which can avoid the effect of the friction between the specimen and the loading device. These measures can ensure a better loading condition and improve the accuracy of testing results.

2.3 Testing results

During the process of loading, the computer automatically recorded the parameters of stress, strain, displacement, pressure, etc. Fig. 4 shows the measurement results of the stress-strain curves for the specimen shown in Fig. 2(a) with the dip angle θ= 15º, 30º and 45º.

For the models with a radial crack emanating from a tunnel roof, as shown in Fig. 1(a), the testing results of the critical stress σ_1 with different crack dip angle θ are shown in Fig. 5 for cement mortar and in Fig. 6 for sandstone. It can be seen that generally, the curve of the average stress σ_1 versus θ for cement mortar is similar to that for sandstone. When crack dip angles θ increase from 0° to 90º, the compressive strength of tunnel models varies remarkably. When θ is 45º, the critical stress of the tunnel model is the lowest, only 8.03 MPa for the cement mortar model, whereas as θ is 0º or 90º, the critical stress of the tunnel models is relatively larger. Testing results of the average critical compressive stress for the cement mortar tunnel models without cracks is 16.03 MPa, which means it is about twice the model with 45º dip angle crack.

For the models with a radial crack emanating from the bottom and sidewall of tunnel models, as shown in Fig. 1(b), the testing results of the critical stress σ_1 with different crack positions are presented in Fig. 7 for cement mortar, and in Fig. 8 for sandstone. Generally, the average stress σ_1 versus crack positions for the two materials are similar. When a crack emanating from tunnel foot, the critical stress is the lowest, only 7.13 MPa, and when a crack emanating from tunnel spandrel, the critical stress of model is also relatively small, 7.85 MPa. Compared to the strength of regular tunnel model without crack, the strength is decreased more than a half, which indicates that the crack emanating from tunnel foot and from tunnel spandrel has a large influence on tunnel stability, and it is necessary to implement further study.

In order to further study the effect of the crack emanating from tunnel foot, experimental study is implemented by using sandstone tunnel models with different dip angle α (from 15° to 255º, with 15° gradient increment) with tunnel bottom, as shown in Fig. 1(c). The testing results of the critical stress σ_1 with different dip angle α are shown in Fig. 9. It can be seen that when crack dip angle α is between 120° and 135º, the critical stress of the tunnel model is the low, which means the corresponding tunnel is prone to damage, and its stability is the low.

3. Numerical study on crack propagation using RFPA code

In order to investigate the crack propagation and

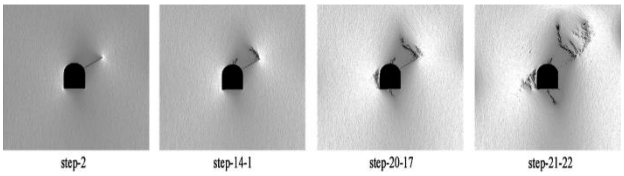

(a) Crack dip angle θ=30°

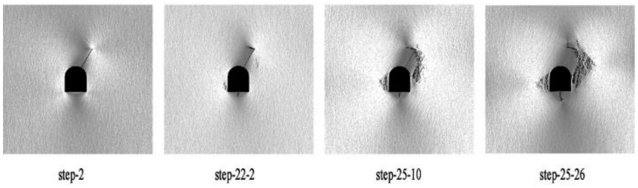

(b) Crack dip angle θ=60°

Fig. 10 Numerical simulation results of crack propagation and damage patterns as a function of time for a tunnel model with a crack emanating from tunnel roof with the dip angle (a) θ= 30° and (b) θ= 60°

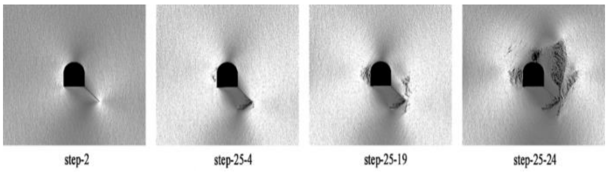

(a) A crack emanating from tunnel foot

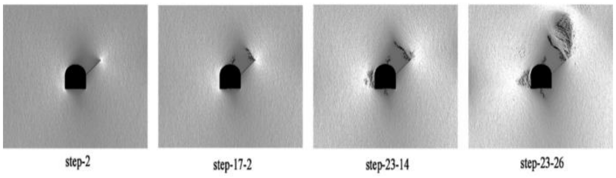

(b) A crack emanating from tunnel spandrel

Fig. 11 Numerical simulation results of crack propagation and damage patterns as a function of time for a tunnel model with a crack emanating from (a) tunnel foot and (b) tunnel spandrel

damage-failure pattern of the tunnel models shown in this experimental study, numerical models are established by using finite element code RFPA (Wang *et al.* 2016b, Yu *et al.* 2016). Because the element in tunnel models may undergo tensile or shear failure, and therefore in this model, two criteria, i.e., maximum tensile strain criterion and Mohr-Coulomb criterion have been applied to judging element stability. According to these two criteria, as the maximum tensile strain or shear stress exceeds the corresponding limit, the element fails. The maximum tensile strain criterion can be written as

$$\varepsilon_1 \leq -\frac{kf_{co}}{E_0} \tag{2}$$

where f_{co} is uniaxial compressive strength (UCS) of an element, k is the ratio of UCS to tensile strength, and E_0 is initial elastic modulus. The Mohr-Coulomb criterion can be expressed as

$$\sigma_1 - \frac{1+\sin\varphi}{1-\sin\varphi}\,\sigma_3 \leq f_{co} \tag{3}$$

where σ_1 and σ_3 are major and minor principal stress, respectively, φ is the internal friction angle. The elastic modulus E will be attenuated after an element is damaged, and it can be expressed as

$$E = (1-\omega)E_0 \tag{4}$$

where ω is damage modulus, E is the elastic modulus after damage.

The numerical models are established based on the tunnel models in this experimental study. A model consists of 250000 elements, and a relatively dense grid is designed near the crack tip in the model. The process of crack initiation, expansion and tunnel damage pattern are simulated. For tunnel models as shown in Fig. 1(a) with a crack dip angle θ=30° and θ=60°, the simulation results of crack propagation and damage process as a function of time are shown in Fig. 10(a) and 10(b), respectively. One can find that damage occurs near crack tip and the damage extent intensifies with crack propagation.

For tunnel models with a radial crack emanating from tunnel foot and tunnel spandrel, the simulation results of crack propagation and damage process as a function of time are shown in Fig. 11(a) and 11(b), respectively. It can be seen that both crack propagation length and the damage extent for the model with a radial crack emanating from tunnel foot is more intense than that emanating from tunnel spandrel.

4. Numerical study using ABAQUS code

In order to further investigate the effect of cracks on tunnel stability, numerical tunnel models are established by using ABAQUS code which was developed based on finite element method, and Tresca stress as well as stress intensity factors are calculated.

4.1 Tresca stress

Tresca stress of tunnel models by using ABAQUE code is acquired, and the results are compared with the failure patterns obtained from numerical simulation using RFPA code and from the model tests in Fig. 12 for tunnel models with different dip angles θ. It can be seen that the model test results generally agree with the numerical simulation results.

For the regular tunnel without cracks, the failure of tunnel model mainly occurs on both sides of tunnel models, and for the models with a radial crack emanating from tunnel roof with different dip angle θ, the tunnel failure mainly occurs around the crack, which means that the cracks do have effect on tunnel stability.

For the tunnel models with a radial crack emanating from the six positions on tunnel edge as shown in Fig. 1(b), the Tresca stress cloud are compared with the model failure patterns obtained from numerical simulation using RFPA code and from tunnel model tests in Fig. 13. One can find that as the crack emanating from the tunnel foot, the Tresca stress around the crack is larger, and the corresponding tunnel damage is more intense.

4.2 Stress intensity factor (SIF) analysis

Stress intensity factors Y_{II} for the tunnel model with

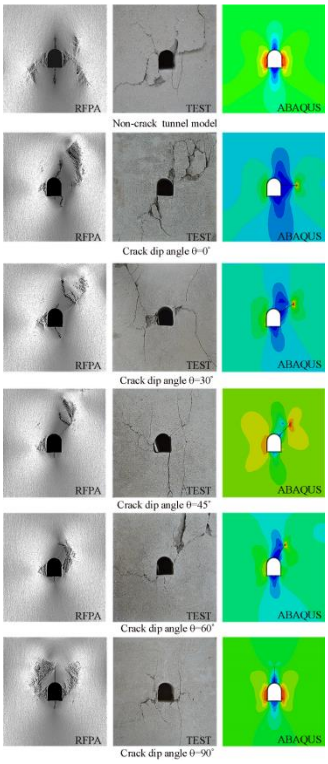

Fig. 12 The Tresca stress cloud images acquired by ABAQUES code and the failure patterns obtained by numerical simulation using RFPA code and from tunnel model tests for the tunnel models with different crack dip angle θ

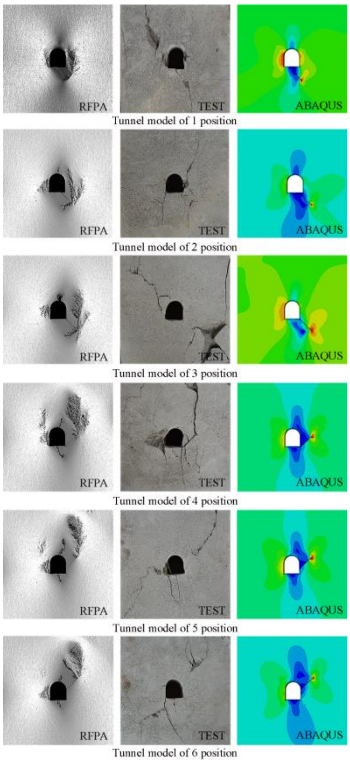

Fig. 13 The Tresca stress cloud images acquired by ABAQUES code and the failure patterns obtained by RFPA code and from tunnel model tests for the tunnel models with a radial crack emanating from different points along tunnel edge

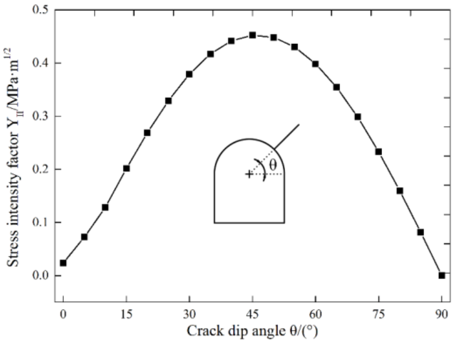

Fig. 14 Dimensionless stress intensity factors Y_{II} for a radial crack emanating from tunnel roof with different dip angle θ

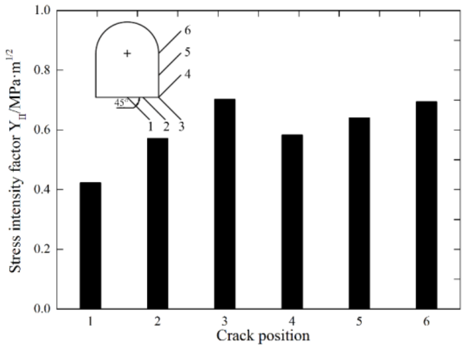

Fig. 15 Dimensionless stress intensity factors Y_{II} for a radial crack emanating from the six points along tunnel edge

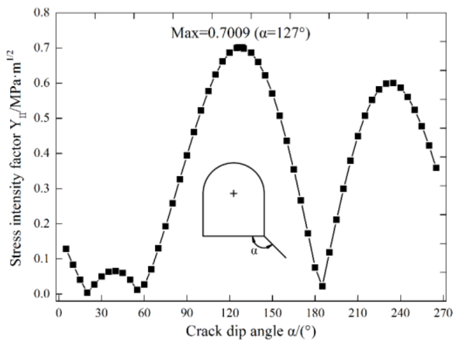

Fig. 16 Dimensionless stress intensity factors Y_{II} for a radial crack emanating from the tunnel foot with different dip angles α

three types of cracks emanating from tunnel edge as shown in Fig. 2 have been calculated by using ABAQUS code, and the results are shown in Figs. 14-16. The calculation results show that the mode I SIF K_I is negative, which means that the cracks under comression will close, and the corresponding crack tips do not have stress concentration. Actually, the compressive load will cause compressive stress at crack tips, which will have a negative effect on crack propagation, but the effect extent of the negative K_I is not clear yet (Zhu 2009a, 2013). Therefore, in this study, the negative K_I is not considered, and only mode II K_{II} is calculated.

For a radial crack emanating from tunnel roof with different dip angle θ as shown in Fig. 2(a), the dimensionless SIF Y_{II} are shown in Fig. 14. It can be seen that as the crack angle θ is 45°, the corresponding Y_{II} value is the largest, which means the corresponding tunnel is the most unstable. The model test results shown in Fig. 5 for cement mortar and in Fig. 6 for sandstone agree well the calculation results of dimensionless SIF Y_{II}; As θ is 0° and 90°, Y_{II} is very small, and the corresponding tunnel is comparatively stable, which can be confirmed from the model test results shown in Figs. 5 and 6.

For the tunnels with a radial crack emanating from the six points on tunnel edge as shown in Fig. 2(b), the dimensionless SIF Y_{II} are shown in Fig. 15. For the crack emanating from tunnel foot numbered position 3, the corresponding dimensionless SIF Y_{II} is the largest, which agrees with the corresponding model test results shown in Fig. 7 for cement mortar and in Fig. 8 for sandstone.

For the tunnels with a radial crack emanating from the tunnel foot with different dip angles α as shown in Fig. 2(c), the dimensionless SIF Y_{II} are shown in Fig. 16. It can be seen that as the crack dip angle α is 127°, the corresponding dimensionless SIF Y_{II} is largest, and as it is 20°, 55° and 185°, the corresponding Y_{II} is small.

Generally, the cracks emanating from tunnel edge do have effect on tunnel stability, and the calculation results of dimensionless SIFs agree with the model test results.

5. Conclusions

Joints or cracks could weaken tunnel stability and it is essential to perform experimental and numerical studies on cracked tunnel failure property so as to obtain a better understanding of the key factors that control tunnel stability. By means of compression tests of tunnel models with a radial crack emanating from tunnel edge and numerical simulation by using two numerical codes, RFPA2D and ABAQUS, the effect of cracks on tunnel stability has been investigated, and the damage-failure mechanism has been analyzed. Through these study, the following conclusions are obtained:

• For tunnel models with a radial crack emanating from tunnel roof as shown in Fig. 2(a), as the dip angle θ is 45°, the mode II stress intensity factor (SIF) Y_{II} is the highest and the corresponding tunnel model has the lowest critical compressive stress, 8.03 MPa (average) for cement mortar tunnel model.

• For tunnel models with a radial crack emanating from tunnel foot as shown in Fig. 2(c), as the dip angle α is 127°, the mode II stress intensity factor (SIF) Y_{II} is the highest and the corresponding tunnel model has the lowest critical compressive stress.

• Generally, for tunnels with a radial crack emanating from three points on tunnel edge, i.e., the middle point between tunnel spandrel and its top with a dip angle 45°, the tunnel foot with a dip angle 127° with tunnel bottom, and the tunnel spandrel with 135° angle with tunnel wall, the corresponding tunnel strength is about a half of the regular tunnel strength and its stability decreases largely.

Acknowledgements

This work was financially supported by the National Natural Science Foundation of China (11672194; 11702181), by Sichuan Administration of Work Safety (aj20170515161307), and by the project of Science and Technology of Sichuan province (2018JZ0036).

References

Baziar, M.H., Nabizadeh, A., Mehrabi, R., Lee, C.J. and Wen, Y.H. (2016), "Evaluation of underground tunnel response to reverse fault rupture using numerical approach", *Soil. Dyn. Earthq. Eng.*, **83**(130), 1-17.

Chen, S.Z. (2014), *The Application of Fracture Mechanics in Highway Tunnel Lining Cracking*, in *Applied Mechanics and Materials*, Trans Tech Publications, 1377-1381.

Dhawan, K., Singh, D. and Gupta, I. (2002), "2D and 3D finite element analysis of underground openings in an inhomogeneous rock mass", *J. Rock Mech. Min. Sci.*, **39**(2), 217-227.

Erdi, A., Zheng, Y.R., Feng, X.T. and Xiang, Y.Z. (2015), "Analysis of circular tunnel stability based on the limit strain method", *Appl. Math. Mech.*, **36**(12), 1265-1273.

Gattinoni, P., Pizzarotti, E.M. and Scesi, L. (2016), "Geomechanical characterisation of fault rocks in tunnelling: The Brenner Base Tunnel (Northern Italy)", *Tunn. Undergr. Sp. Technol.*, **51**, 250-257.

Ghorbani, K., Zahedi, M. and Asaadi, A. (2015), "Effects of statistical distribution of joint trace length on the stability of tunnel excavated in jointed rock mass", *J. Min. Geoeng.*, **49**(2), 289-296.

Gong, Q., Zhao, J. and Jiao, Y. (2005), "Numerical modeling of the effects of joint orientation on rock fragmentation by TBM cutters", *Tunn. Undergr. Sp. Technol.*, **20**(2), 183-191.

Huang, F., Zhu, H., Xu, Q., Cai, Y. and Zhuang, X. (2013), "The effect of weak interlayer on the failure pattern of rock mass around tunnel-scaled model tests and numerical analysis", *Tunn. Undergr. Sp. Technol.*, **35**, 207-218.

Huang, R. and Xiao, H. (2010), "Deformation mechanism of a shallow double-arch tunnel in a sloping rock mass", *Bull. Eng. Geol. Environ.*, **69**(1), 89-97.

Lee, I.M. and Kim, D.H. (2003), "A simulation using a hybrid method for predicting fault zones ahead of a tunnel face", *J. Numer. Anal. Met.*, **27**(2), 147-158.

Li, Y., Zhang, D., Fang, Q., Yu, Q. and Xia, L. (2014), "A physical and numerical investigation of the failure mechanism of weak rocks surrounding tunnels", *Comput. Geotech.*, **61**(3), 292-307.

Liu, J., Li, Y., Xu, S., Xu, S. and Jin, C. (2015), "Cracking mechanisms in granite rocks subjected to uniaxial compression by moment tensor analysis of acoustic emission", *Theor. Appl. Fract. Mech.*, **75**, 151-159.

Mambou, L.L.N., Ndop, J. and Ndjaka, J.M.B. (2015), "Numerical investigations of stresses and strains redistribution around the tunnel: Influence of transverse isotropic behavior of granitic rock, in situ stress and shape of tunnel", *J. Min. Sci.*, **51**(3), 497-505.

Nikadat, N. (2016), "Analysis of stress distribution around tunnels by hybridized FSM and DDM considering the influences of joints parameters", *Geomech. Eng.*, **11**(2), 269-288.

Park, S.W., Park, S.S., Hwang, I.B. and Cha, C.J. (2012), "A case study on cause analysis for longitudinal crack of duct slab in tunnel", *J. Kor. Inst. Struct. Maint. Inspect.*, **16**(5), 19-28.

Satıcı, Ö. and Ünver, B. (2014), "Assessment of tunnel portal stability at jointed rock mass: A comparative case study", *Comput. Geotech.*, **64**, 72-82.

Sun, X., Qiang, Y., Zhao, M.J. and Wang, K. (2013), *Research on Fractal Crack Propagation Mechanism of Hydraulic Tunnel Concrete Lining*, in *Applied Mechanics and Materials*,

TransTech Publications, 1704-1708.
Wang, H., Li, Y., Li, S., Zhang, Q. and Liu, J. (2016a), "An elasto-plastic damage constitutive model for jointed rock mass with an application", *Geomech*. *Eng*., **11**(1), 77-94.
Wang, M., Zhu, Z.M. and Liu, J.H. (2012), *The Photoelastic Analysis of Stress Intensity Factor for Cracks around a Tunnel*, in *Applied Mechanics and Materials*, TransTech Publications, 197-200.
Wang, Q.Y., Zhu, W.C., Xu, T., Niu, L.L. and Wei, J. (2016b), "Numerical simulation of rock creep behavior with a damage-based constitutive law", *J*. *Geomech*., **17**(1), 04016044.
Wang, S.Y., Sloan, S.W., Sheng, D.C., Yang, S.Q. and Tang, C.A. (2014), "Numerical study of failure behaviour of pre-cracked rock specimens under conventional triaxial compression", *J*. *Solid*. *Struct*., **51**(5), 1132-1148.
Yang, X.L. and Yan, R.M. (2015), "Collapse mechanism for deep tunnel subjected to seepage force in layered soils", *Geomech*. *Eng*., **8**(5), 741-756.
Yoo, C. (2016), "Effect of spatial characteristics of a weak zone on tunnel deformation behavior", *Geomech*. *Eng*., **11**(1), 41-58.
Yu, Q., Yang, S., Ranjith, P.G., Zhu, W. and Yang, T. (2016), "Numerical modeling of jointed rock under compressive loading using x-ray computerized tomography", *Rock Mech*. *Rock Eng*., **49**(3), 877-891.
Zhang, Z., Chen, F., Li, N., Swoboda, G. and Liu, N. (2017), "Influence of fault on the surrounding rock stability of a tunnel: Location and thickness", *Tunn*. *Undergr*. *Sp*. *Technol*., **61**(1), 1-11.
Zhu, Z. (2009a), "An alternative form of propagation criterion for two collinear cracks under compression", *Math*. *Mech*. *Solid*., **14**(8), 727-746.
Zhu, Z. (2009b), "Numerical prediction of crater blasting and bench blasting", *J*. *Rock Mech*. *Min*. *Sci*., **46**(6), 1088-1096.
Zhu, Z. (2013), "Evaluation of the range of horizontal stresses in the earth's upper crust by using a collinear crack model", *J*. *Appl*. *Geophys*., **88**, 114-121.
Zhu, Z., Li, Y., Xie, J. and Liu, B. (2015), "The effect of principal stress orientation on tunnel stability", *Tunn*. *Undergr*. *Sp*. *Technol*., **49**, 279-286.

GC